Available online at www.sciencedirect.com
SCIENCE DIRECT®
PERGAMON
Renewable Energy 28 (2003) 1851–1864
RENEWABLE ENERGY
www.elsevier.com/locate/renene

Is AM1.5 applicable in practice? Modelling eight photovoltaic materials with respect to light intensity and two spectra

J.F. Randall *, J. Jacot

Laboratoire de Production Microtechnique, IPR, STI, Ecole Polytechnique Fédérale de Lausanne, CH-1015 Lausanne, Switzerland

Received 6 December 2002; accepted 14 February 2003

Abstract

Solar cell comparison is generally based on an arbitrary maximum terrestrial intensity and spectra (of 1 sun, 1000 W/m^2) at 25 °C perpendicular to the cell plane [1] referred to by specialists as AM1.5. In practice, no solar cell experiences such conditions, yet few alternative bases for comparison exist [2]. Our interest in this paper is to explore the correct design of indoor Photovoltaic (IPV) products. Given that the indoors, when compared with the outdoors, are characterised by much lower radiant energy intensities, various spectra (including artificial light sources), complete comparison data for indoor conditions are not freely available. More general level reports have been published [3–6].

Twenty-one different solar cells representing eight different Photovoltaic material technologies are reproducibly electrically characterised under laboratory based simulated AM1.5 (1 sun; solar spectrum) from 1000 W/m^2 intensity down to the 0.1–1 W/m^2 decade. Some were measured under an artificial light source (fluorescent tube) in the 1–10 W/m^2 decade.

The results are used to validate a phenomenologically based model.

Keywords: Intensity; Photovoltaic technology; Spectra; Survey

* Corresponding author. Tel.: +41-21-693-5945; fax: +41-21-693-3891.
E-mail address: Julian.Randall@epfl.ch (J.F. Randall).

0960-1481/03/$ - see front matter © 2003 Elsevier Science Ltd. All rights reserved.
doi:10.1016/S0960-1481(03)00068-5

Nomenclature

a, b, α, β	constants
AM1.5	air mass 1.5 or standard test conditions [1]
DF	daylight factor (ratio)
E	energy
FF	fill factor
G	intensity
η	efficiency
L	light levels (Lux)
R	resistance

Subscripts

Ext	external
G	band gap
Int	internal
OC	open circuit
P	parallel
Rad	radiant
S	series
SAT	saturation
SC	short circuit

1. Introduction

The inexorable growth in low power micro-electronic devices such as sensors and MEMS (Micro Electro Mechanical Systems) is an opportunity for increasing the use of PV (Photovoltaics) especially for indoor applications. Photovoltaic modules may be used to partially or completely source the energy required for the functioning of such systems. For information, indoor consumer PV represented 4 MW_P in 1997. It is of note that the 1 sun efficiency reference of such statistics is misleading for indoor products, as electrical efficiency is much less important indoors. This is because the end-user decision to purchase an indoor PV (IPV) product is not related to the solar cell electrical efficiency but rather to such benefits as reduced reliance on batteries (”plug and forget”) and increased reliability i.e. a correctly designed and used IPV system can run longer without user intervention than when powered by batteries alone. From an environmental responsibility perspective, reducing battery waste is also laudable.

This paper forms part of a wider project to examine how to extend IPV use beyond the solar calculators and watches to which we are already accustomed. Whilst data

is available to the IPV designer, such as PV materials available, cost, colour, surface areas, 1 sun voltage/current and so on, there remain areas of missing and yet salient information. One of these areas is comparable electrical performance at the light intensities and spectra typical of the indoor environment (< 10 W/m^2 at > 1 m from artificial light source or < 100 W/m^2 at > 1 m from window). Another is a suitable model to predict performance under these conditions. Some comparisons exist for indoor [3–6] and outdoor conditions [7–10]. However, none covers the range of PV technologies, intensities and spectra of this paper.

Using solar cells indoors is both different from outdoors (less variation of temperature, much less intensity {1–10 W/m^2 range rather than 100–1000 W/m^2 range outside}, further spectra, variation of performance with intensity) and similar (importance of cell orientation with respect to radiant energy source/s, impact of obstacles). These issues are more easily understood when one considers those who influence the built environment namely the creators (architects and lighting engineers in the case of IPV) and end-users. Architects when designing in practice try to achieve a balance between a number of factors including safety, cost and comfort (light, temperature, aesthetics, etc.). Chief among these for IPV needs is the light levels which they attempt to maintain as uniform as possible, although this is rarely possible by daylight alone. The reason for this can be seen in Fig. 1, showing typical values of Daylight Factor (DF), which are quite low (a few percent). DF is calculated by the ratio of L_{int}/L_{ext}, where L_{int} and L_{ext} are the light levels in Lux indoors and outdoors respectively. Note the rapid decrease of DF between window and opposite wall to which the human eye adapts imperceptibly.

Lighting engineers aim to fulfil a specification from an architect that complements the daylight component, with the aim of providing whatever artificial lighting will be required. Users are a stochastic element in any system that can be modelled. They can have a significant impact on the available light by the fittings and furniture they require as well as their use-pattern, e.g. how they use lighting and blinds.

These three groups of actors seek a perceived (or photometric) result, whilst PV collects radiant energy. For this paper, the word ‘light’ is used to describe photometric radiation whilst ‘radiant energy’ (E_{rad}) is used for the wider bandwidth radiation to which solar cells are sensitive. Our experiments measuring E_{rad} indoors have confirmed similar trends to those found for light (or DF) shown in Fig. 1.

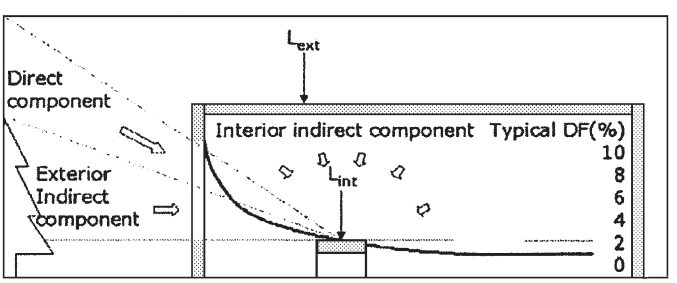

Fig. 1. Daylight factor components and typical values.

In order to increase the range of experiments, simulation can be performed with fewer resources (time, number of sensors, varying less parameters at a time i.e. daylight variation during measurement). The choice of software should be made by prioritising physical accuracy and as such "Radiance"[11] is ideal. The solar cell data presented in this paper when combined with predicted E_{rad} data allow the cumulative charge (Ah) available to be calculated.

Following this section the method used for testing the cells is described (Experimental Procedure) as well as the related findings (Results). In the Model Presentation section, a model is explained and compared with the results. Other issues of interest are reviewed in the Discussion.

2. Experimental procedure

The solar cells were characterised under indoor conditions which departed as little as possible from Standard Test Conditions (STC) [1]. The current/voltage (I/V) characteristics were taken in the standard way for the 21 samples in Table 1 using a Wacom solar simulator as previously described [6]; the E_{rad} intensity was controlled with one or more wire mesh filters between the E_{rad} source and the sample which at maximum filtration reduced the 1000 W/m^2 to approximately 0.8 W/m^2. At each level of intensity, an I/V curve was recorded, as well as the resistances at short circuit, R_{SC} and open circuit, R_{OC}.

Some samples were tested in the same way other than a different light source was used (fluorescent Philips Ecotone PL-L, 830/4P HF, 40 W) to be representative of artificial light sources. The intensity from this source on the solar cell was varied over the 1–5 W/m^2 by controlling the distance ($>$ 1 m range) between the source and the solar cell under test.

The indoor environment typically has a smaller temperature range than outdoors, so all experiments were performed at a fixed temperature (22 °C ± 3). As solar cell efficiency is affected by temperature, this contributed to reducing the uncertainty related to varying more than one variable at a time, often found in outdoor comparative testing [7–10].

3. Results

Samples were accepted from across the quality range from cheap commercial cells up to high performance prototypes. No distinction was made with regard to whether they were designed for indoor or outdoor use. The chief acceptance criterion was that they have an active area suitable for IPV which was taken in this case as being less than 5 cm×5 cm (25 cm^2).

Fig. 2 (left graphs) shows that solar cell efficiency in the highest intensity decade, 100–1000 W/m^2, varies less than in the lower decades. The ranking by 1 sun efficiency is almost completely maintained down to 200 W/m^2. For intensities below 100 W/m^2 (see Fig. 2 right graphs), which are typical of indoor conditions, a much

Table 1
Technologies and sources of the 21 cells tested showing whether the manufacturer was a laboratory or industry, the active area and number of cells in the module of each sample tested

Technological classification	Supplier or laboratory name	Cell code	Indu.=I Labo=L	Active area (cm^2)	No. of cells in module
Silicon (crystalline)	BP Solar (via IWS)	xSi-BP	I	9.36	1
Silicon (crystalline LGBC)	BP Solar, UK	xSi-LGBC	I	0.90	1
Silicon (crystalline)	Spacecells, Edmund Scientific, US	xSi-EdSi	I	0.38	1
Silicon (crystalline)	Unknown (via Distributor)	xSi-Dist	I	10.95	1
Silicon (polycrystalline)	MAIN, TESSAG, D	pSi-MAIN	I	12.47	1
Silicon (polycrystalline)	EFG, TESSAG, D	pSi-EFG	I	10.25	1
Silicon (polycrystalline)	Unknown (via Distributor)	pSi-Dist	I	2.88	1
III-V cells (GaAs)	NREL, Golden, CO, US	3-5-NREL	L	0.25	1
Polycrystalline thin film (CdTe)	Matsushita/ Panasonic, J	CdTe-Mats	I	5.80	5
Polycrystalline thin film (CdTe)	Parma University, I	CdTe-Parm	L	0.79	1
Polycrystalline thin film (CIGS)	ZSW, Stuttgart University, D	CIGS-ZSW	L	0.46	1
Other (GalnP)	NREL, Golden, CO, US	GIP-NREL	L	0.25	1
Amorphous Silicon	TESSAG, Putzbrunn, D	aSi-Tess	I	4.95	5
Amorphous Silicon	Sanyo Electric, Hyogo, J	aSi-Sany	I	3.71	4
Amorphous Silicon	Solems, Paris, F	aSi-Sole	I	1.76	3
Amorphous Silicon	VHF Technologies, Le Locle, CH	aSi-VHF	L	3.36	4
Amorphous Silicon	Sinonar Corporation, Taipei, TW	aSi-Sino	I	1.26	4
Amorphous Silicon	Millenium, BP Solar	aSi-BP	I	0.20	1
Photochemical (Nanocrystalline dye)	Greatcell SA, Yverdon, CH	PC-GCSA	L	1.00	1
Photochemical (Nanocrystalline dye)	EPFL ICP2, Lausanne, CH	PC-ICP2	L	0.90	1
Multijunction cell (GaAs-GalnP tandem)	NREL, Golden, CO, US	MJ-NREL	L	0.25	1

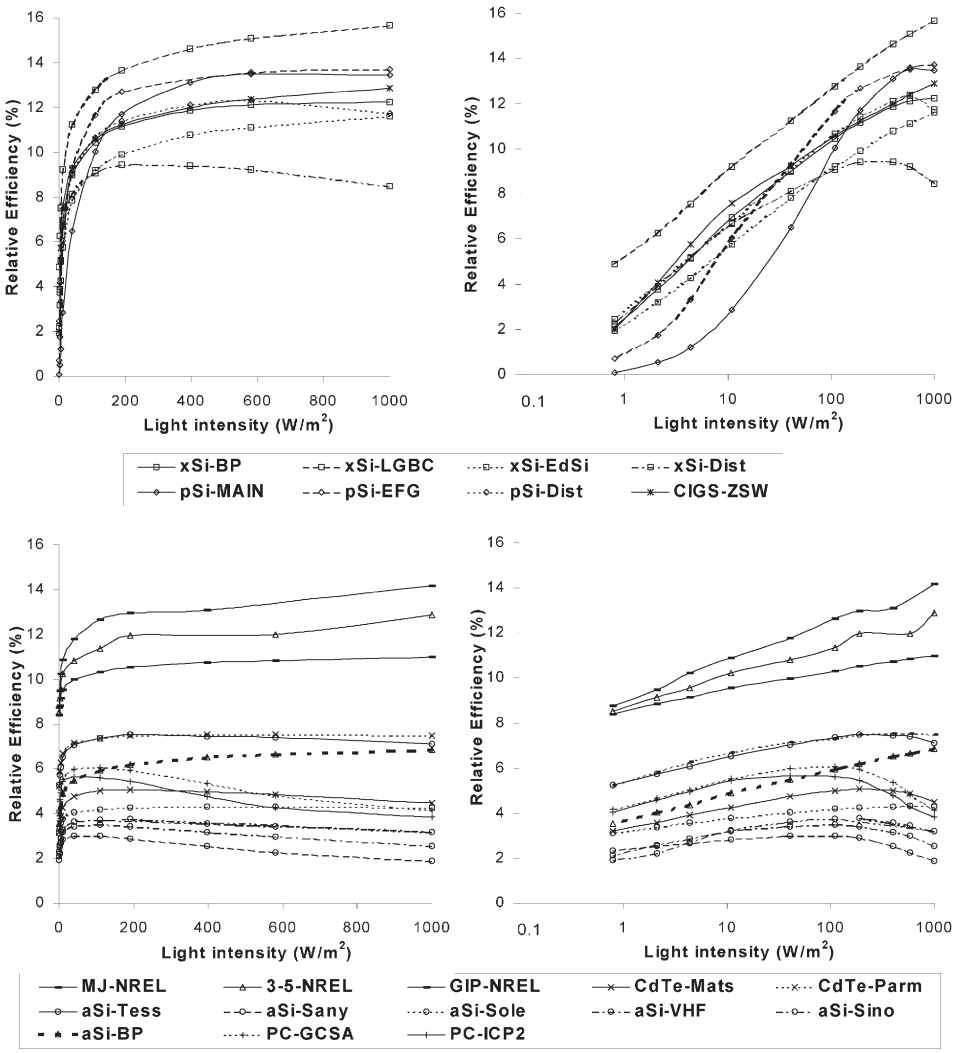

Fig. 2. Efficiency of all samples under wire-mesh filtered AM1.5 (1000 W/m^2) showing same results vs intensity on the base 10 scale (left) and natural logarithm (right). The log scale slope has been used to sort the results between the top and bottom graphs (see phenomenological model).

more marked change is found and the ranking by technology is altered when one reaches the lowest intensities so that some of the highest performing cells at 1 sun were the weakest at 1 W/m^2.

The graphs in Fig. 3 compare the efficiencies under filtered AM1.5 with those found under the fluorescent source for selected samples representing three technologies. The fluorescent intensity was measured using a Lux meter and then converted to W/m^2 using the (simplified) relationship shown in Eq. (1) and Eq. (2).

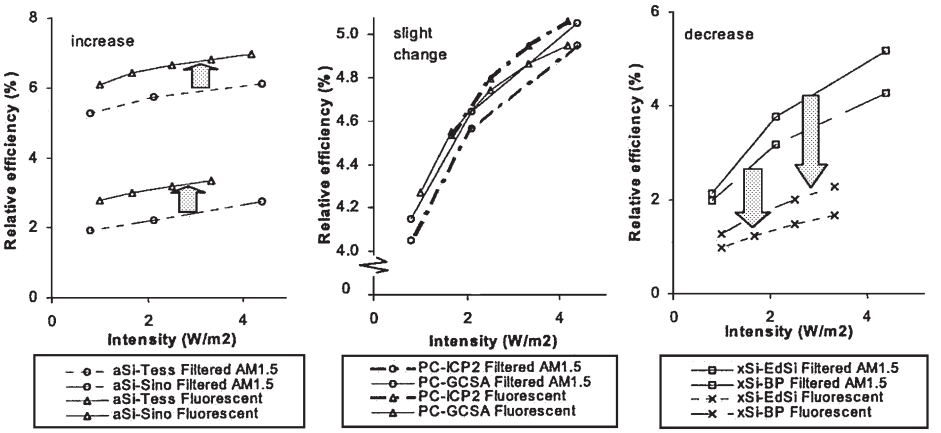

Fig. 3. Efficiency difference going from filtered AM1.5 to the fluorescent spectrum for two samples of three PV technologies: amorphous Silicon single cells (left), dye cell (middle) and crystalline Silicon (right).

$$\frac{E_{\mathrm{rad}}(Lux)}{120{,}000} = \frac{E_{\mathrm{rad}}(W/m^2)}{1000} \tag{1}$$

or:

$$E_{\mathrm{rad}}(W/m^2) = \frac{E_{\mathrm{rad}}(Lux)}{120} \tag{2}$$

4. Model presentation

Efficiency (η) is calculated as follows:

$$\eta = \frac{FF \times I_{SC} \times V_{OC}}{G} \tag{3}$$

where I_{SC} is short circuit current, V_{OC} is open circuit voltage, G is intensity (equal to E_{rad}) and FF (Fill Factor) is the ratio of the maximum power output of the cell to the product of I_{SC} and V_{OC}. For the samples in Fig. 4 it can be seen that FF is approximately constant in the range 1–100 W/m^2. This was found to be relatively valid for all samples, for example the FF maximum–FF minimum for the range 8–100 W/m^2 was 2% for CdTe, 5% for a-Si and dye cells, 22% for poly-crystalline Silicon and 23% for mono-crystalline Silicon. Moreover, it also well known that I_{SC} is directly proportional to G; in this case αG is used instead of I_{SC} where α is a constant:

$$I_{sc} = \alpha G \tag{4}$$

Given that V_{OC} has the following relationship with I_{SC}:

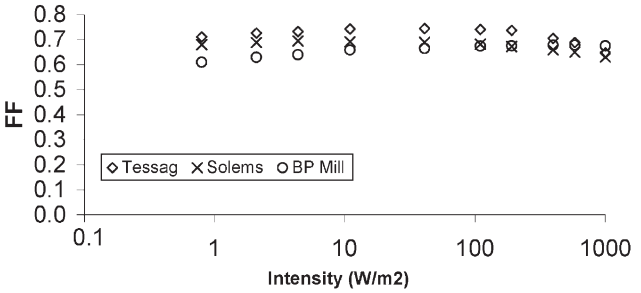

Fig. 4. FF vs Intensity on base 10 log. scale for selected amorphous silicon samples.

$$V_{OC} \cong \frac{kT}{q} \ln\left(\frac{I_{SC}}{I_{SAT}}\right) \tag{5}$$

where I_{SAT} is the saturation current and kT/q is the thermal voltage, substituting Eq. (4) and Eq. (5) into Eq. (3), it can be found that:

$$\eta \cong FF \cdot \alpha \cdot \frac{kT}{q} (\ln G + \ln\alpha - \ln I_S) \tag{6}$$

I_{SAT} can be found [12,13] using the approximate formula in Eq. (7):

$$I_{SAT} \cong \beta \exp\left(-\frac{E_g}{kT}\right) \tag{7}$$

where E_g is the band gap, β is relatively constant and temperature, $T(K)$ is held constant for the experiments, Eq. (6) becomes:

$$\eta \cong FF \cdot \alpha \cdot \frac{kT}{q}\left(\ln G + \ln\alpha - \ln\beta + \frac{E_g}{kT}\right) \tag{8}$$

which in the form:

$$\eta = a \ln G + b \tag{9}$$

has:

$$a = FF \cdot \alpha \cdot \frac{kT}{q} \tag{10}$$

and:

$$b = FF \cdot \alpha \cdot \frac{kT}{q}\left(\ln\alpha - \ln\beta + \frac{E_g}{kT}\right) \tag{11}$$

From the right hand graphs of Fig. 2, it can be seen that the overall trend is a straight line on a logarithmic scale. This is particularly the case in the range 1–100 W/m^2 and for the lower right hand graph. In order to show this more clearly, Fig.

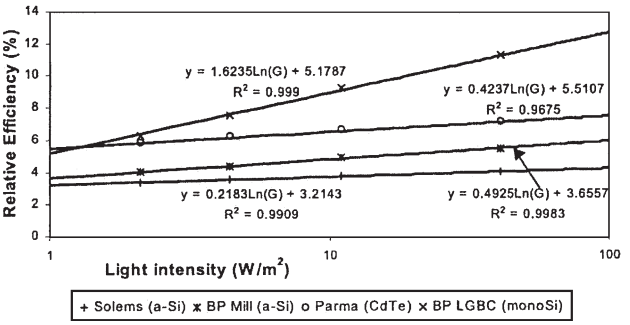

Fig. 5. A magnification of Fig. 2 (r.h.s.) for selected samples compared with the fit of Eq. (9).

5 provides a magnification of the experimental data (points) and their fit with Eq. (9) (lines) over the range 1–100 W/m^2. This latter relationship was applied to the data for all samples in the range 0.8–100 W/m^2 and the results shown in Table 2 suggest a satisfactory fit (average linear correlation coefficient R^2 of 0.98).

An ideal cell for IPV use therefore has as low a value for *a* and as high a value for *b* as possible, as displayed by those samples that perform best in our experiments

Table 2
Phenomenological model (Eq. parameters over in 1–100 W/m^2 range[a]

Cell code	a_{AM}	b_{AM}	R^2	a_{AM}/b_{AM}	~Eg
pSi-EFG	2.33	0.48	0.99	4.87	1.10
pSi-MAIN	2.05	(−)0.84	0.92	2.43	1.10
xSi-EdSi	1.50	2.16	1.00	0.39	1.10
xSi-BP	1.71	2.58	1.00	0.66	1.10
CIGS-ZSW	1.73	2.83	0.98	0.61	0.90
pSi-Dist	1.67	2.80	1.00	0.60	1.10
xSi-Dist	1.40	2.88	0.99	0.48	1.10
xSi-LGBC	1.62	5.18	1.00	0.31	1.10
aSi-Sino	0.40	2.06	0.95	0.19	1.70
aSi-VHF	0.33	2.30	0.96	0.14	1.70
aSi-BP	0.49	3.66	1.00	0.13	1.70
CdTe-Mats	0.38	3.30	1.00	0.11	1.40
PC-IPC2	0.42	4.25	0.95	0.10	–
PC-GCSA	0.40	4.37	0.96	0.09	–
MJ-NREL	0.74	9.02	0.99	0.08	–
aSi-Tess	0.43	5.41	0.99	0.08	1.70
CdTe-Parm	0.42	5.51	0.97	0.08	1.40
aSi-Sany	0.17	2.39	0.98	0.07	1.40
aSi-Sole	0.22	3.21	0.99	0.07	1.40
3-5-NREL	0.57	8.72	0.98	0.07	1.50
GIP-NREL	0.36	8.59	1.00	0.04	1.40

[a] a_{AM} and b_{AM} are values of *a* & *b* under AM1.5 source. Cell codes are defined in Table 1. Average R^2 for all 21 samples is 0.98

under indoor light conditions (e.g. Ga compounds). These two effects can be summarised by altering Eq. (9) as shown in Eq. (12):

$$\eta = b\left(\frac{a}{b}\ln G + 1\right) \tag{12}$$

which gives:

$$\frac{a}{b} = \frac{1}{\ln\alpha - \ln\beta + \frac{E_g}{kT}} \tag{13}$$

Eq. (13) indicates that with α, β and T constant, a/b is inversely related to band gap. In Table 2, the values of a/b are shown for all samples tested. They are ranked by a/b, and although no direct relationship to band gap is found, it can be seen that for a/b greater than 0.3, the approximate material band gap is less than or equal to 1.1. Where a/b is less than 0.2, approximate band gap (where known) is greater than 1.4. This suggests that the latter values of a/b and band gap may be appropriate for IPV; in general, lowest a/b is recommendable for IPV.

Two distinct technological groups are also found when ranking the results with respect to a: those cells with a value of a greater than 1.4 (top eight lines of Table 2, including mono-crystalline Silicon, polycrystalline Silicon and CIGS) and those where a was in the range 0.17–0.74 (lower thirteen lines of Table 2, amorphous Silicon, CdTe, Gallium compounds and dye cells). These two modes have already been identified [6] and this is the first time that numerical variables have been associated with them. However, neither a nor a/b sort cells exactly by band gap. This can be explained not only due to the testing of both cells and modules, but also to the variety of processes and methods used to produce the samples.

Table 3 shows the parameters of Eq. (9) for the results in Fig. 3. These are then compared in Table 4 with the values under AM1.5 (Table 2). As can be seen in Table 4, the amorphous Silicon parameters increase by 13–34%. The dye cell samples parameter b changes little and have an 18–36% increase in parameter a. The crystalline Silicon samples parameters decrease from 51–67%. This indicates that the latter

Table 3
Phenomenological model parameters for 1–100 W/m^2 under the fluorescent source[a]

Cell code (see Table 1)	a_F	b_F	R^2	a_F/b_F
xSi-BP	0.82	1.26	1.00	0.65
xSi-EdSi	0.57	0.95	1.00	0.60
aSi-Sino	0.46	2.76	1.00	0.17
aSi-Tess	0.57	6.11	1.00	0.09
PC-IPC2	0.57	4.26	1.00	0.13
PC-GCSA	0.48	4.29	0.99	0.11

[a] a_F and b_F are values of a & b under fluo. source. Average R^2 for all 6 samples is 1.00

Table 4
The ratio of fluorescent parameters (Table 3) to AM1.5 parameters (Table 2)

Cell code (see Table 1)	a_F/a_{AM}	b_F/b_{AM}
xSi-BP	0.48	0.49
xSi-EdSi	0.41	0.33
aSi-Sino	1.15	1.34
aSi-Tess	1.32	1.13
PC-IPC2	1.36	1.00
PC-GCSA	1.18	0.98

samples are affected more by spectral mismatch (product of the incident spectrum and the spectral response of the cell integrated over the response range) than the amorphous and dye cells.

5. Discussion

The effect of series resistance (R_S) and parallel (shunt) resistance (R_P) on solar cell I/V curves is known [13], see equivalent circuit in Fig. 6 and modelled [14]. At high E_{rad} intensity, high R_S reduces *FF* whilst at low E_{rad}, low R_P reduces *FF*. The effect of R_S and R_P on efficiency can be seen in the gradient of the curves in Fig. 2. This is consistent with the hypothesis [15] that where R_S is sufficiently high that the shunt current is negligible, then efficiency below 1 sun will first increase as radiant energy intensity is reduced. As can be seen, some samples in the intensity decade 100–1000 W/m^2 have such a negative gradient. Where the gradient approaches zero, the efficiency is maximised. For IPV products in particular, knowledge of these efficiency variations can improve product and cell design as well as help to explain variations in performance of ostensibly similar modules.

As a complement to the results, it would be interesting to test further cell samples, especially of those technologies which are not as well represented here (e.g. CIGS) and those that performed well at low light levels, such as CdTe and the Gallium compounds. This would allow further scrutiny and improvement of the model

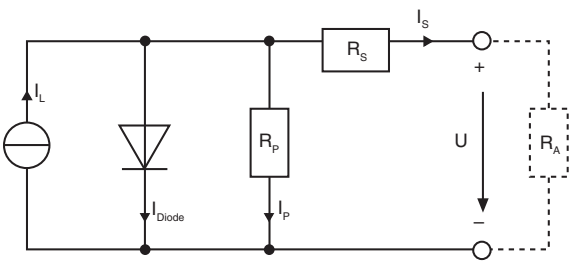

Fig. 6. Equivalent circuit of Photovoltaic solar cell or module.

presented. An ideal outcome from the IPV practitioner perspective would be a model based on easily accessible data (such as 1 sun efficiency) which would provide a prediction of cell performance over the full range of intensities tested here. The phenomenological model (Eq. (8)) is valid for only some of the samples across the full range tested, 0.8–1000 W/m^2, namely Solems, BP Millenium and Tessag. In order to extend the validity, more terms are required to model that part of the efficiency-intensity curve where the gradient becomes negative. It is also necessary to investigate the physical meaning of the control parameters a (Eq. (10)) and b (Eq. (11)).

Another area requiring better understanding is the physical mechanism which induces R_P. Assuming it is not dependent on light intensity, the R_P at low light intensities can be related to efficiency. R_P was estimated by taking the R_{SC} for a selection of samples at a low E_{rad} (4.4 W/m^2). Fig. 7 suggests that there is a natural log relationship between R_P and efficiency per technology.

The effect of incident radiant energy spectrum is of interest for the IPV practitioner. It has been demonstrated in Fig. 3 that amorphous Silicon sample efficiency was higher with fluorescent spectrum (up 14–34% at 2 W/m^2) whilst the crystalline Silicon samples efficiency deteriorated (down 51–57% at 2 W/m^2) compared with filtered AM1.5. It would be interesting to test other samples as well as corroborate the results with comparison of the spectral response. The latter was not pursued, as the selection of samples did not include a single cell sample (a pre-requisite for the spectral response equipment) for each technology.

For those interested in developing IPV products, other factors apart from PV design are important. Ideal products that can benefit from PV power perform datalogging and/or sensor functions. This is because their functionality is only required in intermittent spikes separated by relatively long ‘rest’ periods such as Fig. 8.

The main charge consumption need is therefore the standby current, which unfortunately for many present IC designs can be of the order of mA rather than the μA typically produced indoors by PV. The development of ever more efficient microcontroller standby/sleep modes is important for PV penetration in indoor products.

Most IPV products require charge storage to allow use when E_{rad} is too low. A

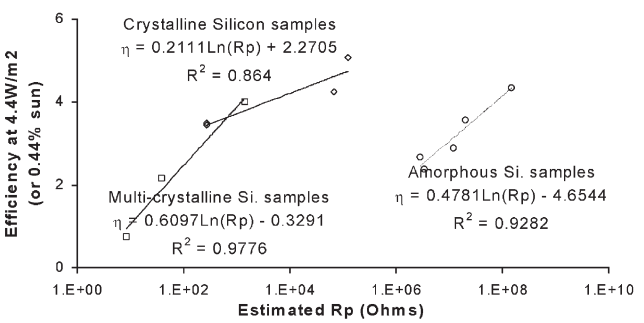

Fig. 7. R_{SC} (approx. R_P) vs efficiency under low illumination (4.4 W/m^2 filtered AM1.5).

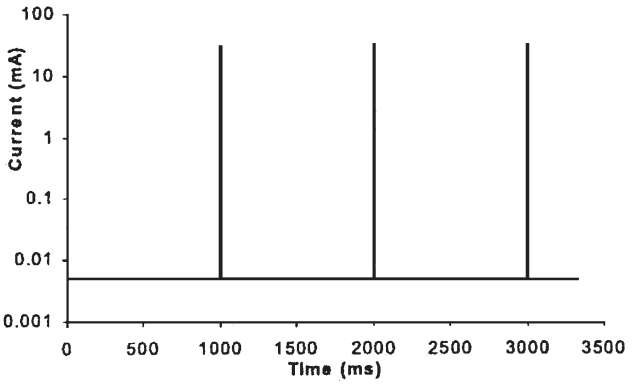

Fig. 8. Typical charge consumption of datalogging or sensor device.

number of charge storage technologies are available, one of which (RAM™) is well adapted to IPV due to its low rate of self-discharge (see Fig. 9).

Further aspects of IPV design that should be considered include final appearance, solar cell orientation with respect to the E_{rad} source(s) as well as a number of module design parameters such as cell width [16].

6. Conclusion

At the beginning of this paper, the lack of comparable low intensity solar cell data was mentioned. This gap has been partly filled by the results presented here for 21 samples representing eight technologies tested under two spectra types. These show that efficiency is not constant with intensity, technology and spectra.

Also the reasons why existing solar cell comparisons e.g. [1] are not applicable

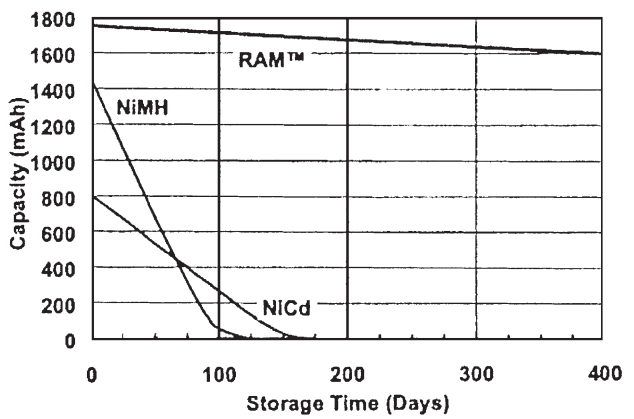

Fig. 9. Secondary cell self-discharge technology comparison, courtesy Battery Technologies Inc., CAN.

for indoor PV (IPV) design have been presented. For example, absolute efficiency may vary markedly with intensity in the decades 1–100 W/m^2 (see Fig. 2).

The lack of appropriate models has also been identified; two forms of a phenomenologically based model have been shown to correlate well to experimental results in the intensity range of interest for IPV design.

This paper has identified a number of issues important to IPV design and has provided results that may contribute to better resolving them.

Acknowledgements

W. Durisch (PSI, CH), G. Leyland, M-O. Hongler, F. Dusonchet (all three at EPFL, CH) and E. Meyer (University of Port Elizabeth, South Africa) are thanked for helpful discussion. We are grateful to C. Droz (University of Neuchatel, CH), R. Gottschalg (CREST, UK), S. Kurtz (NREL, CO., USA) and D. Baetzner (LSSP, Zurich, CH) for corrections. Above all, our thanks to all those who provided samples.

References

[1] IEC-904-3, *IEC Standard* i.e. 1000 W/m^2 AM1.5 normal to cell surface at 25 °C, 1989.
[2] Bücher K. Solar Energy Materials and Solar Cells 1997;47:85–94.
[3] Roth W, Schmid J. 8th EC Photovoltaic Solar Energy Conference. p. 263–9.
[4] Pettersson H, et al. Electronics Goes Green 2000+, Berlin. p. 735–9.
[5] Nakajima H. JEE, June 79. p. 26–9.
[6] Randall JF, et al. 17th EPVSECE, Munich, 2001.
[7] Camani M, et al. 2nd World Conf. and Ex. on PVSEC. 6–10 July 1998, Vienna.
[8] Eikelboom JA, Jansen MJ. ECN report ECN-C-00-067, June 2000.
[9] Anderson D, Bishop J, Dunlop E. 16th EPVSECE 1–5 May 2000, Glasgow, UK.
[10] Chianese D, et al. 16th EPVSECE 1–5 May 2000, Glasgow, UK.
[11] Software available on 31.1.02 via http://radsite.lbl.gov/radiance/HOME.html.
[12] Möller HJ. Semiconductors for solar cells. Artech, 1993. p. 29, Equation 2.39.
[13] Green M. Solar cells operating principles, NSW, 1982. p. 88.
[14] Oritz-Conde A, et al. Solid-State Electronics 2000;44:1861–4.
[15] Meyer EL. MSc Thesis, Uni. of Port Elizabeth, South Africa, Chap. 3, p. 15–30.
[16] Burgleman M, Niemegeers A. Sol. En. Mat. and Sol. Cells 1999;57:85–95.